Using data to attribute episodes of warming and cooling in instrumental records

Ka-Kit Tung[1] and Jiansong Zhou

Department of Applied Mathematics, University of Washington, Seattle, WA 98195

Edited by Robert E. Dickinson, University of Texas at Austin, Austin, TX, and approved December 26, 2012 (received for review July 20, 2012)

The observed global-warming rate has been nonuniform, and the cause of each episode of slowing in the expected warming rate is the subject of intense debate. To explain this, nonrecurrent events have commonly been invoked for each episode separately. After reviewing evidence in both the latest global data (HadCRUT4) and the longest instrumental record, Central England Temperature, a revised picture is emerging that gives a consistent attribution for each multidecadal episode of warming and cooling in recent history, and suggests that the anthropogenic global warming trends might have been overestimated by a factor of two in the second half of the 20th century. A recurrent multidecadal oscillation is found to extend to the preindustrial era in the 353-y Central England Temperature and is likely an internal variability related to the Atlantic Multidecadal Oscillation (AMO), possibly caused by the thermohaline circulation variability. The perspective of a long record helps in quantifying the contribution from internal variability, especially one with a period so long that it is often confused with secular trends in shorter records. Solar contribution is found to be minimal for the second half of the 20th century and less than 10% for the first half. The underlying net anthropogenic warming rate in the industrial era is found to have been steady since 1910 at 0.07–0.08 °C/decade, with superimposed AMO-related ups and downs that included the early 20th century warming, the cooling of the 1960s and 1970s, the accelerated warming of the 1980s and 1990s, and the recent slowing of the warming rates. Quantitatively, the recurrent multidecadal internal variability, often underestimated in attribution studies, accounts for 40% of the observed recent 50-y warming trend.

multidecadal variability | solar influence | Little Ice Age | Maunder Minimum

The world's longest instrumental record of temperature, Central England Temperature (CET), began to be collected in 1659 in an area enclosed by Lancashire, London, and Bristol, a few years after the invention of sealed liquid thermometers. It is the only instrumental record that extends back to the Little Ice Age (LIA), a period of cold climate in Europe, and the time of the Maunder Minimum, when sunspots vanished almost entirely for 70 y (1). The record then covers several subsequent episodes of natural and anthropogenic warming of multidecadal durations. Manley (2) painstakingly compiled most of the early monthly CET series, and Parker et al. (3) the daily data from 1772. Both are updated to present by the Met Office Hadley Centre. This record has previously been analyzed to study interannual and interdecadal variability up to the 25-y period (4); interannual winter variability and its association with solar forcing (5); and its variance at interannual, interdecadal timescales compared with a general circulation model output (6). The lower frequency portion of the record, longer than 50 y, has not been adequately analyzed, the difficulty being that even this long record is not long enough to avoid the cone of influence from the edges of the time series. Here we use a statistical approach to quantify the edge effects. It is this low-frequency portion of the record that contains information about an important multidecadal mode of variability that extends into the modern, industrial era. Wu et al. (7, 8) pointed out the importance of this mode in the modern global temperature record with a period of 65 y: If it is interpreted as natural and related to the Atlantic Multidecadal Oscillation (AMO) (9–12), then the trend attributed to anthropogenic warming should be significantly reduced after ~1980, when the AMO was in a rising phase. However, if it is forced by time-varying aerosol loadings, it should properly be interpreted as part of an accelerating anthropogenic trend. We argue that the former is true, using information from the preindustrial era.

Fig. 1 shows the Continuous Wavelet Spectrum of CET as a function of frequency and time. It can be seen that there is a highly statistically significant band of oscillation with periods of 50–80 y extending throughout the 353-y record, which coincides with the global-mean HadCRUT4 (14) spectrum (Fig. S1), which is also statistically significant. We will not discuss the oscillation that has a longer average period of 90–100 y because it cannot be properly confirmed by the global-mean record, which is too short for our statistical test. There is, additionally, an oscillation in the 30- to 40-y band that is nonstationary: it exists only during the 19th century when the 50- to 80-y band is temporarily weak. There is little power in this higher frequency band in the global-mean data available after 1850. It is likely that this higher frequency band represents local information along the Atlantic coast and will not be discussed further here, except to point out that one definition of the AMO Index, by Trenberth and Shea (15), tends to emphasize this regional effect for the purpose of aiding the prediction of Atlantic hurricanes by subtracting the global-mean temperature from the North Atlantic mean. We will use the standard AMO Index of Enfield et al. (16), which is defined as the North Atlantic mean sea-surface temperature (SST), linearly detrended.

The original time series can be reconstructed from the wavelet transform and divided into several frequency bands (13) (Fig. S2). It can be verified that these "band-filtered" data, when summed, give back the original CET time series.

The 50-y low-pass filtered time series (containing the wide frequency band with periods longer than 50 y) is shown in Fig. 2 with the global mean from HadCRUT4, similarly low-passed, superimposed. It is seen that CET agrees quite well with the global-mean data. Both datasets contain a multidecadal oscillation that is statistically significant at above the 95% confidence level (Fig. 1 and Fig. S1). This result is important because the statistical significance of this multidecadal oscillation in the long records has not been established previously either in Greenland ice core data (17) or in a previous analysis of CET (18). The 50- to 90-y band (which is approximately the same as the 50- to 80-y band) is here referred to as the "AMO" mode and is shown in Fig. 3*A*. The CET's AMO agrees well with both the global and the North Hemispheric (NH) mean surface temperature, showing that the AMO is a near-global phenomenon. The NH mean is slightly larger than the global mean. The closeness of the global mean and

Author contributions: K.-K.T. and J.Z. designed research; J.Z. performed research; J.Z. contributed new reagents/analytic tools; K.-K.T. and J.Z. analyzed data; and K.-K.T. wrote the paper.

The authors declare no conflict of interest.

This article is a PNAS Direct Submission.

[1]To whom correspondence should be addressed. E-mail: ktung@uw.edu.

This article contains supporting information online at www.pnas.org/lookup/suppl/doi:10.1073/pnas.1212471110/-/DCSupplemental.

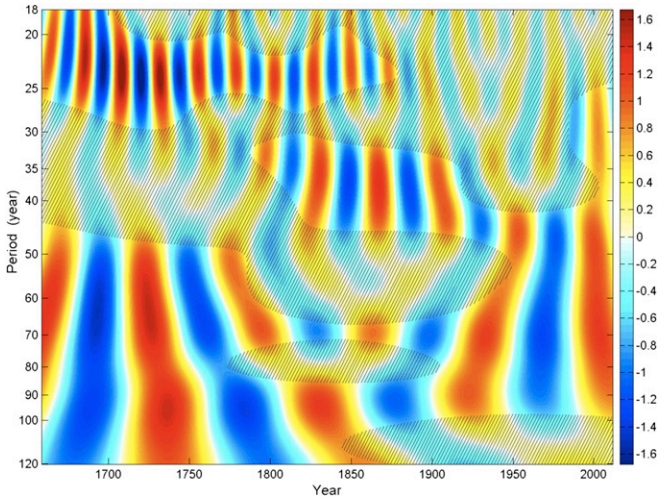

Fig. 1. Continuous wavelet spectrum of CET. Wavelet coefficient [calculated using equation 2 of Torrence and Compo (13)] is shown as a function of period and time, using a Morlet wavelet with the parameter chosen to emphasize time resolution. Regions below the 95% confidence level are hatched. The statistical test is based on an autogressive of order 1, AR (1), noise model. The formula used is the χ^2 test (13).

the NH mean before the early 20th century may be due to the lack of data south of 60° S. The AMO should be out of phase in the region of the Antarctic circumpolar ocean (21), where deep water from the North Atlantic upwells. The global-mean oscillation exhibits a peak-to-peak amplitude of about 0.3–0.4 °C with an average period of about 70 y, based on its recent cycles.

AMO

CET is regional data. Although it has been a common practice in studying paleoclimate data to use proxy data from, for example, an ice core in Antarctica, to represent global climate after dividing the former by a factor of ~2 or by a model-determined, latitude-dependent scaling factor, theoretical justification is only beginning to be emphasized (22). The present finding that the low-frequency portion of the regional data agrees with the global mean (with a scaling that is slightly larger than 1) during the 162-y overlap period supports the notion (but does not prove) that a single time series can, in fact, be used to represent the global mean variation. To validate the CET time series for the preindustrial era in its ability for near-global representation, we use the multiproxy data of Delworth and Mann (12), which has near-global coverage (Fig. 3*B*). Before 1850, the CET AMO agrees with this multiproxy data in phase, ~~and~~ the amplitudes in the proxy data are only relative. The spatial pattern of this multidecadal variability in the multiproxy data is similar to that in the recent global instrumental record—a monopole with emphasis on the North Atlantic region extending to the Pacific and North American region (23, 24). However, after 1850, there is a gradual divergence in time of the multiproxy record from the global instrumental record. This is well recognized, but the cause is unclear (25). CET, being an instrumental record, does not suffer such a divergence. England, being near the Atlantic coast, is strongly influenced by the Atlantic sea-surface temperature. Indeed, Fig. 3*B* shows that CET coincides with the often used AMO Index (16) over the past 150 y. We therefore argue that CET can be used as a proxy AMO index, extending the latter back to 1659. The amplitude of the global AMO in the preindustrial era can also be calibrated against the CET AMO. Wood et al. (20) considered a 200-y record of surface air temperature reconstructed from four stations in the Atlantic–Arctic boundary. Their undetrended data are shown in Fig. 3*C* and compared with CET data. The phases of the oscillations in the two data sets are in agreement. The amplitude of the Arctic data is larger due to polar amplification. The extra years before 1850 coincided with the weaker AMO cycle shown in the middle cycle of the CET AMO. Without the benefit of seeing the earlier cycles shown in Fig. 3, Wood et al. conjectured that the early 20th-century warming is a singular internal variability event without a regular period.

Using 800 y of ice-core data from Greenland, Broecker (26) in 1975 extracted two recent cycles of an oscillation by combining an 80-y Fourier harmonic with a 180-y harmonic and correctly predicted the end of cooling in the 1970s and the ensuing decades of accelerating warming. Neither harmonic, however, is statistically significant in his record. Gray et al. (27) considered tree-ring–based reconstruction of the AMO back to 1567. However, the cycle earlier than CET has an unusually large excursion; the tree rings may have been contaminated by the severe cooling during the Little Ice Age, caused likely by the very large volcano explosions. Chylek et al. (17) examined five ice-core datasets in Greenland for the overlapping period of 1303–1961 and reported finding two timescales for the AMO, a 20-y and a 45- to 85-y oscillation. Although the 20-y spectral peak was found to be statistically significant, the lower frequency oscillation that we are interested in was found to be below statistical significance, due possibly to the spectral windowing used. Wu et al. (8), using global-mean data, revealed a statistically significant 2.5 cycles with a 65-y period. DelSole et al. (28) also found 2.5 cycles by extracting the spatial pattern in the Intergovernmental Panel on Climate Change, Fourth Assessment Report (IPCC AR4) (29) model control runs that best characterizes internal variability and by projecting the observed global data onto this pattern. Wu et al. (8), DelSole et al. (28), and Delworth and Mann (12) related the global-mean oscillation to a spatial pattern emphasizing the North Atlantic, with Pacific and global extensions. The five cycles found here argue that this oscillation is primarily natural and recurrent (10). The phenomenon likely involves thermohaline circulation variability in the Atlantic Ocean. As described in refs. 30 and 31, the oscillation is the result of negative feedbacks between the strength of the thermohaline circulation that brings warm SST to the North Atlantic and the Arctic ice melt in response to the warm SST. With reduced deep-water formation, the latter then slows the thermohaline circulation after a delay of 20 y. Recently a 55- to 80-y AMO has been model-simulated as arising from the variability of the meridional overturning circulation in the Atlantic (32). Using CET as supporting evidence, we have shown here that these same 2.5 cycles in the global data are a part of a recurrent oscillation going back at least 350 y, and ~~therefore~~ it is unlikely that they can be attributed to volcanic aerosols, whose eruptions were not periodic nor aligned with the troughs (Fig. 3*A*).

Booth et al. (33) simulated AMO-like variability in the 20th century with time-varying aerosol forcing, incorporating its indirect effect. However, Zhang et al. (34) showed that they overestimated the indirect aerosol effect. The vertical subsurface temperature in the tropical Atlantic should have a characteristic anticorrelation pattern with the upper ocean in the observed AMO, but is not produced in Booth et al. (33) (see also ref. 35). Although it may be possible to simulate half of a cycle (i.e., the early 20th-century warming) using time-varying anthropogenic aerosols within their uncertainty, it is very unlikely that they can be the cause of the five cycles found here.

Climate Variation Since the LIA

Fig. 2 shows almost four centuries of climate variations recorded in CET. First, we note that the record can be divided into three eras, consisting two perturbed climates—the rapid warming after the end of LIA and the modern period of anthropogenic warming after the Second Industrial Revolution—separated by a background climate when Europe experienced a century (1738–1849) of mild temperature with no trend. (See also the objectively

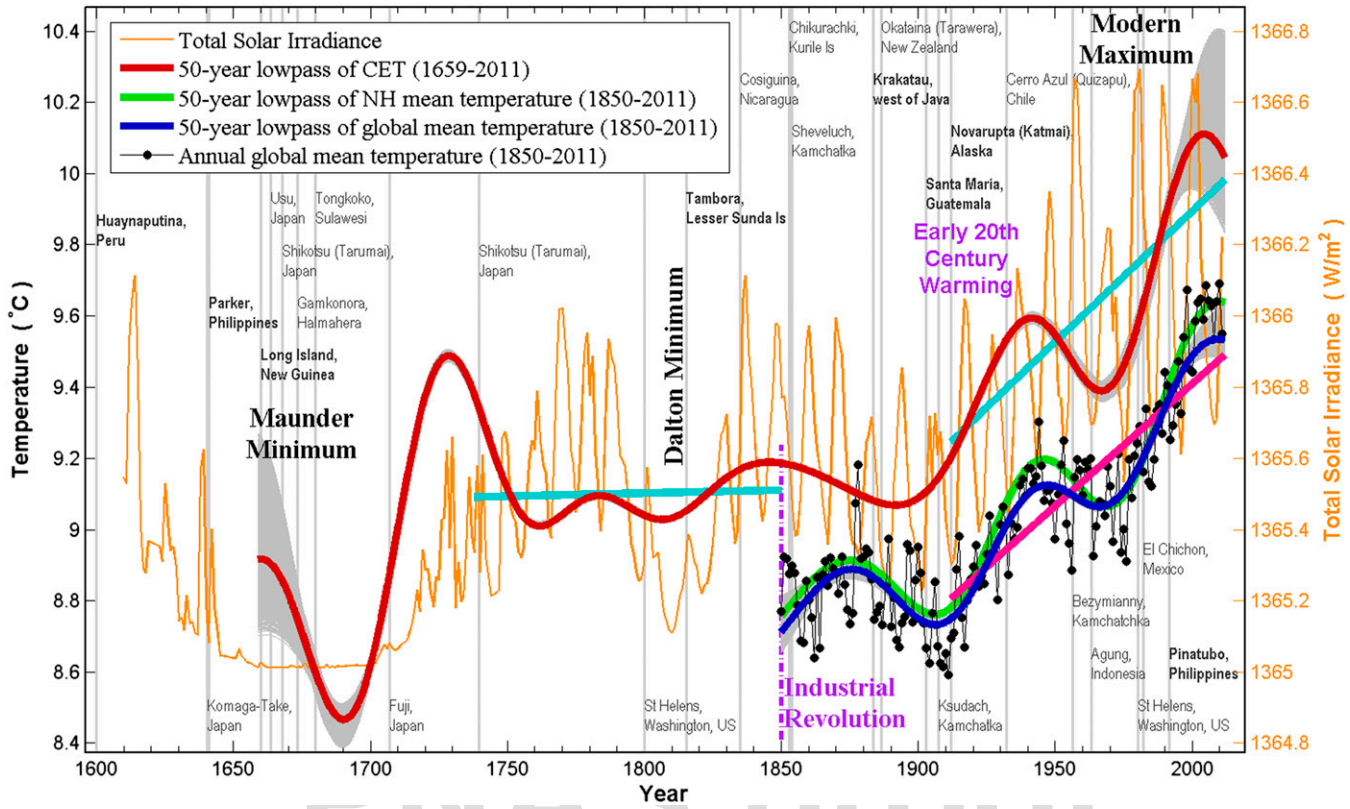

Fig. 2. Four centuries of climate variation. The low-frequency portion of the monthly Central England Temperature, in red, is calculated using the 50-y low-passed filtered wavelet reconstruction. Similarly constructed global mean temperature is shown in blue and North Hemispheric mean in green, offset by the fact that HadCRUT4 data are relative to the 1960–1999 mean. The raw annual mean data are shown in the background for the global mean. Light-blue straight lines are least-squares fit to selected periods in CET. It shows that there is a century after 1750 with little trend and that the recent 100-y trends in the CET and global mean (pink straight line) are approximately the same. The thin gray curves are from 3,000 synthetic time series, which have 2^{14} −1 mo added to each side of the same 1659–2011 information. The gray band quantifies the errors due to the cone of influence (edge effects). TSI (scale on the right axis), courtesy of Judith Lean, is shown in orange. Years of large volcano eruptions [with a Volcano Explosivity Index (VEI) of 5 and higher] are indicated by light-gray vertical lines. Boldface type is used for the names of major volcano eruptions with a VEI of 6 and 7.

deduced secular trend in Fig. S2.) This separation renders the persistent speculation that the current global-warming trend is a continued "rebound" from the cold of LIA (36) unlikely. The rebound ended in 1750.

The presence of multidecadal internal variability superimposed on the secular trend gives the appearance of accelerated warming and cooling episodes at roughly regular intervals. Below we give a consistent explanation of the four centuries of climate variation based on the assumption that much of the AMO is natural and recurrent.

Almost no sunspots were observed during a 70-y interval (1645–1715) called the Maunder Minimum (1). Large volcano eruptions—Huaynaputina (1600), Parker (1641), and Long Island (1660)—contributed to the cold LIA at the beginning of the CET record. An unusual series of five large volcano eruptions from 1660 to 1680 probably prolonged the cold into the Late Maunder Minimum. A negative phase of the AMO accentuated the cold further in Late Maunder Minimum, reported in Europe (1), although it was thought that the cold CET was only "locally representative" (37). Our current work argues that it is probably global because the AMO has in-phase global manifestations (Fig. 3). There were no major known volcanoes from 1680 to 1707 [although there were some unknown ones (38)], and it started to warm. Although commonly attributed to the Sun (1), the rapid warming of ∼1 °C at the end of Maunder Minimum is 10 times greater than our understanding of the solar radiation change (39) can explain but is within the range of a speculative theory (40) if we remove 0.4 °C as due to the AMO. The timing of the warming, however, appears to precede the increase in total solar irradiance (TSI) (39, 41) by 20–30 y and favors the reduced volcanic aerosol loading as the main cause for the warming—the rebound. The 20-y small dip in temperature near 1810 coincides with the solar Dalton Minimum, but is probably caused by a negative excursion of the AMO. The rising AMO cycle in the first half of the 19th century produced a warming, despite the eruption of Tambora (1815), the largest in the past four centuries. The next rising phase of AMO (7, 8, 26, 28) led to the often cited early 20th-century warming in the global mean (1910–1940) of 0.4 °C (Fig. 2), but it happened to occur during a period of increasing mean solar irradiance, leading some to attribute it, incorrectly, to solar forcing (42). The observed warming rate for that period lies above the range of all model responses to combined anthropogenic and natural forcing compiled by IPCC AR4 (29), even after correcting for a discontinuity in the wartime data (43), corroborating the suggestion here that it is mostly caused by internal variability. The cooling experienced in the 1960s and 70s is seen as occurring in the negative phase of the AMO. The period after the 1970s shows a secular increase in global-mean temperature. The rising AMO half-cycle gives the appearance of an accelerated warming that lasted until 2005 (discounting the warm El Niño of 1998). Recently, there have been debates about the slowing of the warming rates since 2005, with explanations (44–46) ranging from increases in stratospheric water vapor and background aerosol to increased coal burning in the emergent economy of China of the past 20 y. If one accepts the conclusion that the AMO is recurrent, and because this period

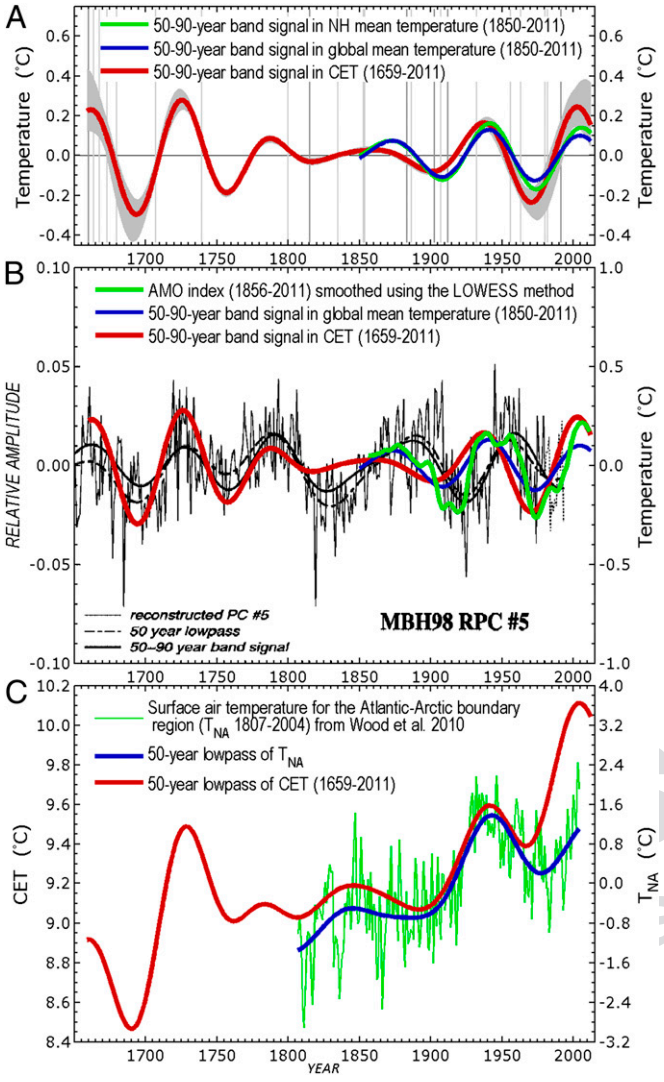

Fig. 3. AMO mode. (*A*) The multidecadal variability (50- to 90-y wavelet band-passed) in CET (in red), in global-mean temperature (in blue), and in Northern Hemisphere mean (in green), using HadCRUT4 are compared. The light-gray curves are the corresponding band pass of 3,000 synthetic data obtained by random resampling of 200-y blocks of CET data to extend the record before 1659 and after 2011. To show that the troughs of the AMO are not systematically aligned with large volcano eruptions, years of large volcano eruptions (with a VEI of 5 and higher) are indicated by light-gray vertical lines, with darker-gray lines for major volcano eruptions with a VEI of 6 and 7. (*B*) The CET AMO is compared with the AMO from the multiproxy data (12). The AMO Index (16) smoothed by locally weighted scatterplot smoothing (LOWESS) (19) is superimposed (in green). The LOWESS is a modified running-time mean, and its use allows the mean to extend to the beginning and end of the record. It uses quadratic fit to 25-y subintervals. It shows that the CET's AMO agrees with the AMO Index and with the global mean after 1850 and agrees in phase with the multiproxy data in the preindustrial period. (*C*) The raw temperature data in the Atlantic–Arctic boundary (not detrended) (in green) from Wood et al. (20), courtesy of Brian Smoliak, and its 50-y wavelet low pass (blue). The low-pass CET is shown in red.

coincides with the start of the descending phase of the AMO, one can suggest that the AMO is a more likely explanation.

Solar and Volcanic Contributions to Global Warming

The solar contribution to the 50-y linear trend is minimal simply because the trend in solar forcing for the past 50 y is minimal (39, 47) (Fig. 2). The debate on satellite calibration yielding an upward trend (48) in the TSI has been settled in favor of no trend in the satellite era (49). Before the satellite era, solar models differ on the degree of irradiance increase. After reviewing these solar models in light of additional evidence on facular areas, Foukal (50) ruled out the possibility of a rapid brightening of the Sun that is required to produce the early 20th-century warming. Without relying on a solar model, we attempted to deduce the solar signal using observed terrestrial response only. The procedure should include non-TSI solar effects, such as from galactic cosmic rays. We (47) found the spatial fingerprint for the combined 11-y solar cycle and secular solar trend after the global-warming trend was removed cycle by cycle while allowing solar-related changes between cycles. The observed temperature was projected onto this pattern to yield a response to both cyclic and secular solar forcing. TSI information was used only for the classification of solar maximum and solar minimum. For the first half of the 20th century, the solar contribution to the linear trend was less than 10%. It does not support the much larger role (>50%) for the Sun in the observed warming, obtained by Scafetta and West (42) by attributing early 20th-century warming to solar forcing (see also ref. 51). The observed solar-cycle response suggests that it is a response to radiative effects of the TSI, amplified by the same climate feedback factors as for the greenhouse radiative forcing (52, 53). There were no consecutive large volcanic eruptions in the 20th century, and none that could have caused the recent slowdown in the rate of global warming.

Global Warming in HadCRUT4 Data

We are now in a position to quantitatively attribute the warming in the global data. Two different approaches are used to show consistency, given the importance of the result. Various fitted linear trends in global-mean temperature up to 2005 were presented in the IPCC AR4 (54), with the recent 25-y trend (at 0.177 °C/decade) larger than the 50-y trend (0.128 °C/decade), which is in turn larger than the 100- and 150-y trends (0.074 and 0.045 °C/decade, respectively). The result is updated to 2011 in Fig. 4*A*. The phenomenon of "accelerating warming trends" is still present. The fitted 25-y trend is not robust, being sensitive to the addition or subtraction of a single-year end-point datum and so will not be discussed further here. A 50-y wavelet low-pass filter is applied to the data points. It is seen by eye that the smoothed curve captures the main episodes of warming and cooling in the past 162 y that are present in the raw data as it agrees with the simple running mean. In particular, one can see that there is a low-frequency oscillation present in the data. We reprocess the data after removing the oscillatory component, defined by the 50- to 90-y wavelet band, the AMO. The removal of the AMO in the determination of the anthropogenic warming trend is justified if one accepts our previous argument that this multidecadal variability is mostly natural. Linear trends are then fitted to the resulting data points in Fig. 4*B* in the same way as in the IPCC AR4. It is visually apparent in Fig. 4*B* that removing the oscillatory AMO from the raw data organizes the data points into a monotonic band and yields a more stable linear trend, converging to the 50-y trend of 0.08 °C/decade. We argue that this is the long-term anthropogenic trend, forced by greenhouse gas increases offset by tropospheric aerosol cooling, which also increased along with industrialization. Comparing Fig. 4*B* with Fig. 4*A*, we see that the internal variability accounts for 40% of the observed 50-y trend. This is essentially the conclusion of Wu et al. (8).

Foster and Rahmstorf (55) considered the period 1979–2010 and obtained an estimate of anthropogenic warming after removing the El Niño-Southern Oscillation (ENSO), individual volcanic eruptions, and the solar forcing through multiple regression analysis. Their adjusted data also showed no change in the linear warming rate over the period, but their estimate for anthropogenic warming, at 0.17 °C/decade for HadCRUT3v, is twice as high as ours. The oscillatory component of AMO, which happens to be in a positive half-cycle, appears as a positive trend in their data since 1979. This

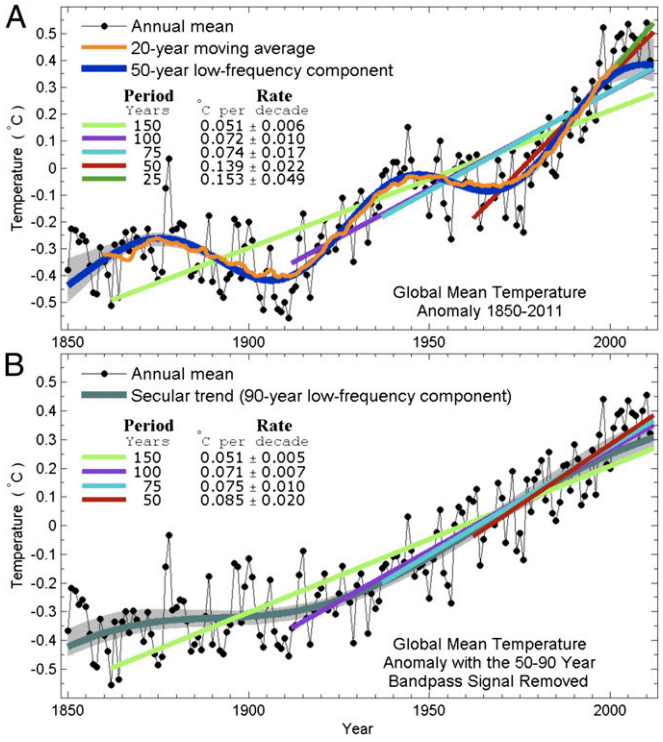

Fig. 4. Understanding global-mean trends. (*A*) The result in IPCC AR4 is updated using HadCRUT4 from 1850 to 2011, and their 150-, 100-, 50-, and 25-y linear trends (with labeled magnitudes) are shown. Even though the annual means are shown, the linear trends are calculated using the raw monthly-mean data. The 50-y wavelet low-passed global mean is superimposed (in blue). It gives a smoothed fit to the raw data and agrees with the running-time mean (in orange). (*B*) The black dots represent adjusted annual-mean global-mean temperature data with the 50- to 90-y wavelet band removed. The removed band is shown in Fig. 3. The linear trends are recalculated. Although the 150-y trend is the same as in *A*, trends for the shorter periods are reduced and become more stable. The 90-y low-pass data (in dark green) is the secular trend for the 162-y period, showing a slow start of the anthropogenic warming in the first 50 y and an almost constant warming trend after 1910. The thin gray curves are the 90-y low pass of 3,000 Monte-Carlo synthetic data of 37,000 mo long, obtained by random resampling in 100-y blocks for the purpose of quantifying the edge effect.

is demonstrated in Fig. 5, where Foster and Rahmstorf's analysis is repeated, but for the longer period of 1856–2011 and using HadCRUT4. The residual plus the regressed linear trend is shown in Fig. 5*A*. The same anthropogenic trend since 1979 of 0.17 °C/decade is obtained. However, one can see clearly that a 70-y oscillation is still present in the residual (see the orange running mean). In Fig. 5*B*, we add the AMO Index (16) to the multiple linear regression analysis. The 33-y net anthropogenic warming rate obtained, at 0.07 °C/decade, is less than half of Foster and Rahmstorf's. In fact, the net anthropogenic warming trend has been remarkably steady for the past 100 y at 0.07–0.08 °C/decade. Further discussions of the multiple regression analysis can be found in Zhou and Tung (56).

Conclusion

Although there is a competing theory that the observed multidecadal variability is forced by anthropogenic aerosols during the industrial era (33), our present work showing that this variability is quasi-periodic and extends at least 350 y into the past with cycles in the preindustrial era argues in favor of it being naturally recurrent and internally generated. This view is supported by model results that relate the variability of the global-mean SST to North Atlantic thermohaline circulation (30, 31, 35) and by the existence of an AMO-like variability in control runs without anthropogenic forcing (28). If this conclusion is correct, then the following interpretation follows: The anthropogenic warming started after the mid-19th century of Industrial Revolution. After a slow start, the smoothed version of the warming trend has stayed almost constant since 1910 at 0.07–0.08 °C/decade. Superimposed on the secular trend is a natural multidecadal oscillation of an average period of 70 y of significant amplitude of 0.3–0.4 °C peak to peak, which can explain many historical episodes of warming and cooling and accounts for 40% of the observed warming since the mid-20th century and for 50% of the previously attributed anthropogenic warming trend (55). Because this large multidecadal variability is not random, but likely recurrent based on its past behavior, it has predictive value. Not taking the AMO into account in predictions of future warming under various forcing scenarios may run the risk of overestimating the warming for the next two to three decades, when the AMO is likely in its down phase.

Methods

The time series was first linearly detrended, and a modulated annual cycle of an average period of 1 y was removed in the wavelet 9- to 15-mo band (the second mode in Fig. S2). This procedure does not affect the wavelet spectrum but is needed for the statistical test. In Fig. 2, the trend is added back.

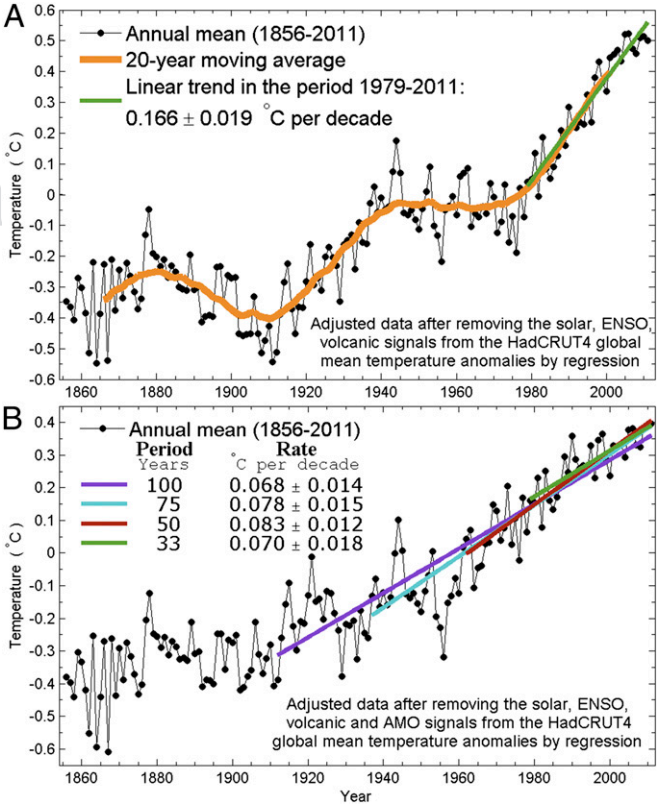

Fig. 5. Multiple-regression analysis of global-mean temperature, (*A*) Adjusted data after the removal of ENSO, volcano, and solar influence. Time lags for ENSO and volcano are 4 and 6 mo, respectively, determined by optimizing the goodness of fit. A running-time mean (in orange) shows a long-period oscillation still present in the residual. (*B*) Adjusted data after the removal of ENSO, volcano, and solar influence, plus the AMO. The AMO index (16) is shown in Fig. 3. The correlation between solar secular forcing trend and the global forcing trend is not small, and so there is a concern of collinearity in the regressors in this method, but the influence on the results is negligible. The noise model used in the multiple linear regression is AR (p), with $p = 4$ for *A* and $p = 2$ for *B*. The error bar for linear least squares fit is ±2 SDs.

We assume that the missing past and future data have similar spectral shape and autocorrelation as the available data. A synthetic time series, as long as desired with the real observations residing in the middle, can be produced using the so-called moving-block bootstrap method (57). We generated a large number of synthetic monthly time series to mimic the natural temperature data over a long period of 37,002 mo. Trend removal from each data block was first performed to reduce artificial oscillations resulting from the discontinuous trends between blocks. These blocks are time-reversed when used to create the future data to avoid large discontinuities at 2011. The least-squares linear trend and its upper and lower 95% confidence limits are taken out, separately, from the central part of each synthetic time series, to account for the influence of the regression errors in the wavelet analysis, and then added back after band pass of the wavelet modes. These form the range of possible edge errors, replacing the common method of showing the cone of influence in the wavelet spectrum without quantifying the range of errors. Other ways of generating the synthetic data, such as using a seasonal autoregressive integrated moving average noise model, produce smaller error bars.

ACKNOWLEDGMENTS. We thank Drs. Zhaohua Wu and Norden Huang for discussions on empirical mode decomposition and trend. We benefitted from comments by John M. Wallace, Isaac Held, and Dennis Hartmann on various versions of this manuscript. The research is supported by the National Science Foundation under Grants ATM 808375 and DMS 0940342 and by the National Aeronautics and Space Administration under Grants NNX11AC75G and NNH10ZDA001N-LWSTRT.

1. Eddy JA (1976) The maunder minimum. *Science* 192(4245):1189–1202.
2. Manley G (1974) Central England temperatures: Monthly means 1659 to 1973. *Q J R Meteorol Soc* 100(425):389–405.
3. Parker DE, Legg TP, Folland CK (1992) A new daily central England temperature series, 1792–1991. *Int J Climatol* 12(4):317–342.
4. Plaut G, Ghil M, Vautard R (1995) Interannual and interdecadal variability in 335 years of central England temperatures. *Science* 268(5211):710–713.
5. Lockwood M, Harrison RG, Woollings T, Solanki SK (2010) Are cold winters in Europe associated with low solar activity? *Environ Res Lett* 5(2):1–7.
6. Karoly D, Stott PA (2006) Anthropogenic warming of central England temperature. *Atmos Sci Lett* 7:81–85.
7. Wu Z, Huang NE, Long SR, Peng CK (2007) On the trend, detrending, and variability of nonlinear and nonstationary time series. *Proc Natl Acad Sci USA* 104(38):14889–14894.
8. Wu Z, Huang NE, Wallace JM, Smoliak B, Chen X (2011) On the time-varying trend in global-mean surface temperature. *Clim Dyn* 37:759–773.
9. Folland CK, Palmer TN, Parker DE (1986) Sahel rainfall and worldwide sea temperatures. *Nature* 320:602–606.
10. Knight JR, Allan RJ, Folland CK, Vellinga M (2005) A signature of persistent natural thermohaline circulation cycles in observed climate. *Geophys Res Lett* 32:L20708.
11. Schlesinger ME, Ramankutty N (1994) An oscillation in the global climate system of period 65–70 years. *Nature* 367(6465):723–726.
12. Delworth TL, Mann ME (2000) Observed and simulated multidecadal variability in the Northern Hemisphere. *Clim Dyn* 16:661–676.
13. Torrence C, Compo GP (1998) A practical guide to wavelet analysis. *Bull Am Meteorol Soc* 79(1):61–78.
14. Morce CP, Kennedy JJ, Rayner NA, Jones PD (2012) Quantifying uncertainties in global and regional temperature change using an ensemble of observational estimates: The HadCRUT4 data set. *J Geophys Res* 117(D8), 10.1029/2011JD017187.
15. Trenberth KE, Shea DJ (2006) Atlantic hurricanes and natural variability in 2005. *Geophys Res Lett* 33:L12704.
16. Enfield DB, Mestas-Nunez AM, Trimble PJ (2001) The Atlantic multidecadal oscillation and its relation to rainfall and river flows in the continental U. S. *Geophys Res Lett* 28(10):2077–2080.
17. Chylek P, Folland CK, Dijkstra HA, Lesins G, Dubey MK (2011) Ice-core data evidence for a prominent near 20 year time-scale of the Atlantic Multidecadal Oscillation. *Geophys Res Lett* 38:L13704.
18. Baliunas S, Frick P, Sokoloff D, Soon W (1997) Time scales and trends in the central England temperature data (1659–1990): A wavelet analysis. *Geophys Res Lett* 24(11): 1351–1354.
19. Cleveland WS, Devlin SJ (1988) Locally weighted regression: An approach to regression analysis by local fitting. *J Am Stat Assoc* 83(403):596–610.
20. Wood KR, Overland JE, Jonsson T, Smoliak BV (2010) Air temperature variations on the Atlantic-Artic boundary since 1802. *Geophys Res Lett* 37:L17708.
21. Chylek P, Folland CK, Lesins G, Dubey MK (2010) Twentieth century bipolar seesaw of the Arctic and Antarctic surface air temperatures. *Geophys Res Lett* 37:L08703.
22. North GR, Wang J, Genton MG (2011) Correlation models for temperature fields. *J Clim* 24(22):5850–5862.
23. Mann ME, Bradley R, Hughes MK (1998) Global-scale temperature patterns and climate forcing over the past six centuries. *Nature* 392(6678):779–787.
24. Delworth T, Greatbatch RJ (2000) Multidecadal thermohaline circulation variability driven by atmospheric surface flux forcing. *J Clim* 13(9):1481–1495.
25. Briffa KR, et al. (1998) Reduced sensitivity of recent tree-growth to temperature at high northern latitudes. *Nature* 391(6668):678–682.
26. Broecker WS (1975) Climatic change: Are we on the brink of a pronounced global warming? *Science* 189(4201):460–463.
27. Gray ST, Graumlich LJ, Betancourt JL, Pederson G (2004) A tree-ring based reconstruction of the Atlantic Multidecadal Oscillation since 1567 A.D. *Geophys Res Lett* 31:L12205.
28. DelSole T, Tippett MK, Shukla J (2011) A significant component of unforced multidecadal variability in the recent acceleration of global warming. *J Clim* 24(3):909–026.
29. Solomon S, et al. (2007) *Climate Change 2007: Working Group I:The Physical Science Basis* (Cambridge, UK), pp 996.
30. Dima M, Lohmann G (2007) A hemispheric mechanism for the Atlantic Multidecadal Oscillation. *J Clim* 20(11):2706–2719.
31. Semenov VA, et al. (2010) The impact of North Atlantic-Arctic multidecadal variability on Northern Hemisphere surface air temperature. *J Clim* 23(21):5668–5677.
32. Wei W, Lohmann G (2012) Simulated Atlantic Multidecadal Oscillation during the Holocene. *J Clim* 25(20):6989–7002.
33. Booth BBB, Dunstone NJ, Halloran PR, Andrews T, Bellouin N (2012) Aerosols implicated as a prime driver of twentieth-century North Atlantic climate variability. *Nature* 484(7393):228–232.
34. Zhang R, et al. (2013) Have aerosols caused the observed Atlantic Multidecadal variability? *J Atmos Sci*, 10.1175/JAS-D-12-0331.1.
35. Zhang R (2007) Anticorrelated multidecadal variations between surface and subsurface tropical North Atlantic. *Geophys Res Lett* 34:L12713.
36. Akasofu S (2010) On the recovery from the Little Ice Age. *Nat Sci* 2(11):1211–1224.
37. Jones PD, et al. (2009) High-resolution palaeoclimatology of the last millennium: A review of current status and future prospects. *Holocene* 19(1):3–49.
38. Gao C, Robock A, Ammann C (2008) Volcanic forcing of climate over the past 1500 years: An improved ice core-based index for climate models. *J Geophys Res* 113(D23), 10.1029/2008JD010239.
39. Wang Y-M, Lean J, Sheeley NR, Jr. (2005) Modeling the Sun's magnetic field and irradiance since 1713. *Astrophys J* 625(1):522–538.
40. Foukal P, Ortiz A, Schnerr R (2011) Dimming of the 17th century sun. *Astrophys J Letters* 733:L38.
41. Lean J, Rottman GJ, Harder J, Kopp G (2005) SORCE contributions to new understanding of global change and solar variability. *Sol Phys* 230:27–53.
42. Scafetta N, West BJ (2005) Estimated solar contribution in the global mean surface warming using ACRIM TSI satellite composite. *Geophys Res Lett* 32:L18713.
43. Thompson DWJ, Kennedy JJ, Wallace JM, Jones PD (2008) A large discontinuity in the mid-twentieth century in observed global-mean surface temperature. *Nature* 453(7195):646–649, 10.1038/nature06982.
44. Solomon S, et al. (2010) Contributions of stratospheric water vapor to decadal changes in the rate of global warming. *Science* 327(5970):1219–1223.
45. Solomon S, et al. (2011) The persistently variable "background" stratospheric aerosol layer and global climate change. *Science* 333(6044):866–870.
46. Kaufmann RK, Kauppi H, Mann ML, Stock JH (2011) Reconciling anthropogenic climate change with observed temperature 1998–2008. *Proc Natl Acad Sci USA* 108(29): 11790–11793.
47. Zhou J, Tung KK (2010) Solar-cycle response in 150 years of sea-surface temperature. *J Clim* 23(12):3234–3248.
48. Scafetta N, Willson R (2009) ACRIM-gap and TSI trend issues resolved using a surface magnetic flux TSI proxy model. *Geophys Res Lett* 36:L05701.
49. Gray LJ, et al. (2010) Solar influences on climate. *Rev Geophys* 48:RG4001.
50. Foukal P (2012) A new look at solar irradiance variation. *Sol Phys* 279(2):365–381.
51. Benestad RE, Schmidt GA (2009) Solar trends and global warming. *J Geophys Res* 114(D14), 10.1029/2008JD011639.
52. Cai M, Tung KK (2012) Robustness of dynamical feedbacks from radiative forcing: 2% solar versus 2 x CO2 experiments in an idealized GCM. *J Atmos Sci* 69(7):2256–2271.
53. Zhou J, Tung KK (2013) Observed tropospheric temperautre response to 11-year solar cycle, and what it reveals about mechanisms. *J Atmos Sci* 70(1):9–14.
54. Trenberth KE, et al. (2007) *Climate Change 2007: The Physical Science Basis*, ed Solomon S (Cambridge Univ Press, Cambridge, UK), pp 235–336.
55. Foster G, Rahmstorf S (2011) Global temperature evolution 1979–2010. *Environ Res Lett* 6(4):1–8.
56. Zhou J, Tung KK (2013) Deducing the multi-decadal anthropogenic global warming trend using multiple regression analysis. *J Atmos Sci* 70(1):3–8.
57. Wilks DS (1997) Resampling hypothesis tests for autocorrelated fields. *J Clim* 10(1): 65–82.

Supporting Information

Tung and Zhou 10.1073/pnas.1212471110

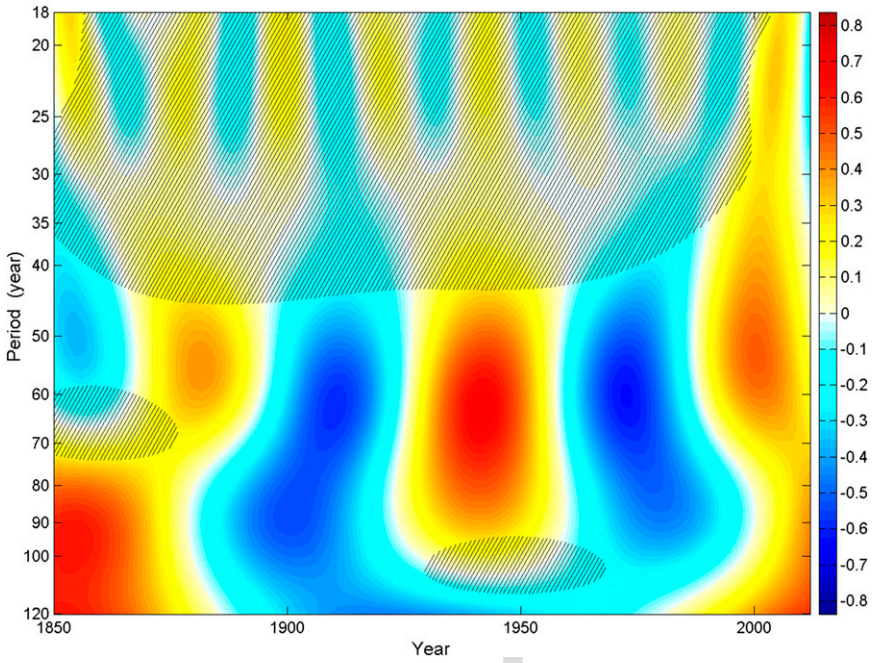

Fig. S1. Wavelet spectrum of the global mean HadCRUT4 temperature, 1850–2011. The hatched areas are below 95% confidence level.

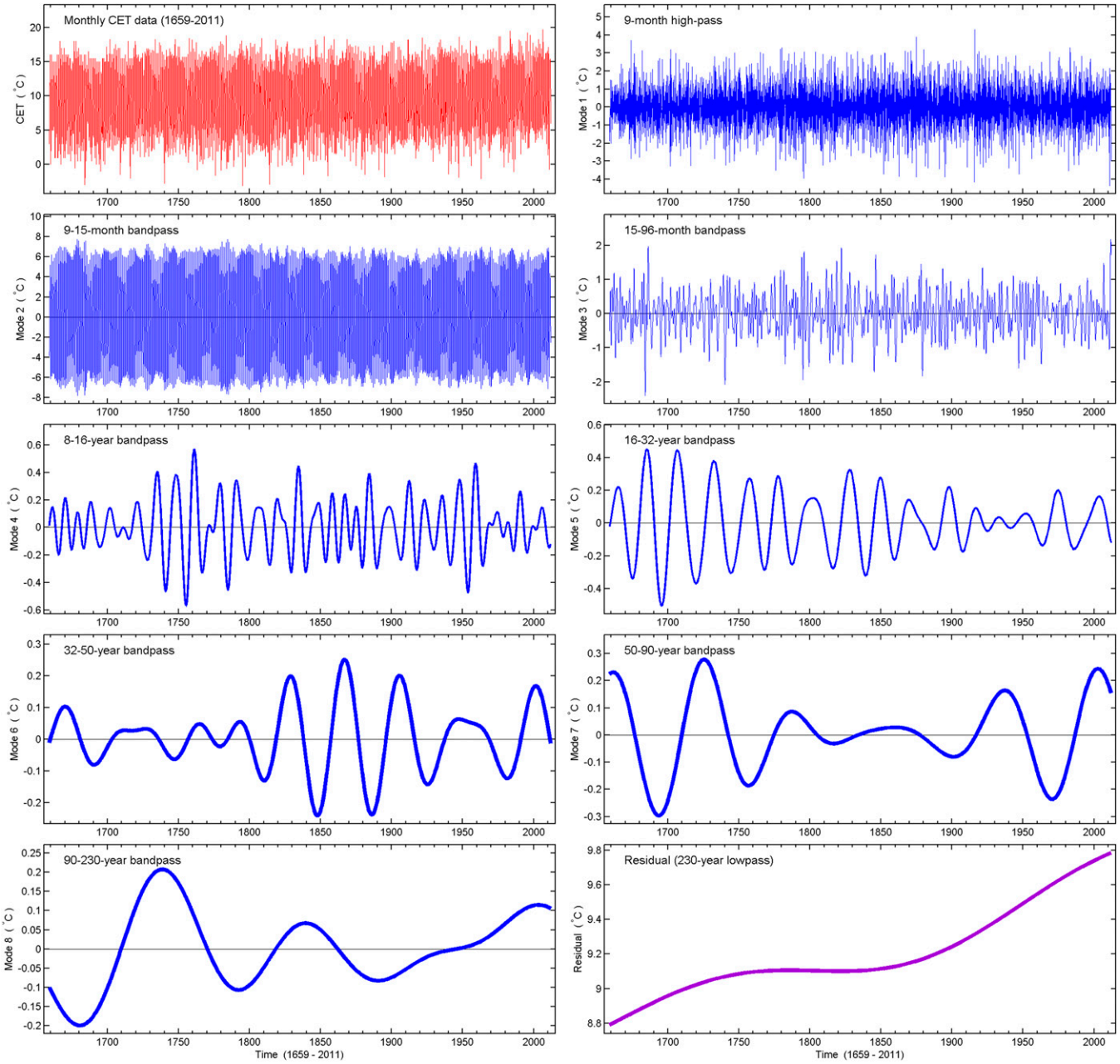

Fig. S2. Wavelet reconstruction of the original time Central England Temperature series is shown in the first panel. The other panels are various band-filtered parts that together reconstruct the original data.